Fe^{3+} center in ZnO

R. Heitz, A. Hoffmann, and I. Broser
Institut für Festkörperphysik, Technischen Universität Berlin, Hardenbergstrasse 36, D-1000 Berlin 12, Germany
(Received 3 December 1991)

In the spectral region around 690 nm, a richly structured luminescence is observed in undoped high-quality ZnO crystals. By means of emission, excitation, and magneto-optical spectroscopy, this luminescence is unambiguously assigned to the $^4T_1(G)$-$^6A_1(S)$ transition of isolated Fe^{3+} ions on Zn^{2+} lattice sites. Basic arguments are the sixfold degeneracy of the ground state with an isotropic g factor of 2.020 ± 0.015, a long lifetime of 25.2 ms, and the fine structure of the $^6A_1(S)$ ground state. The observed fine structure of the excited $^4T_1(G)$ state indicates an intermediate Jahn-Teller coupling instead of the strong coupling usually observed for isoelectronic centers in II-VI and III-V compound semiconductors. The excitation mechanism is described by an energy transfer to Fe^{2+} centers by free holes. The holes are photogenerated at deep acceptors with ionization energies above 2.25 ± 0.05 eV. The $^4T_1(G)$-$^6A_1(S)$ transition energy is found to shift $+39\pm3$ μeV/nucleon by an isotope effect induced by Fe isotopes and to shift 365 and 222 μeV, respectively, by the presence of one ^{18}O ion among the ^{16}O ions of the $Fe^{3+}O^{2-}{}_4$ cluster, depending on its location. The isotope shifts are interpreted in the framework of mass-dependent local modes, which contribute to the total energy of the transition-metal states. Here, the Jahn-Teller interaction as well as the C_{3v} distortion of the $Fe^{3+}O^{2-}{}_4$ cluster is taken into account.

I. INTRODUCTION

In most semiconductors, $3d$-transition-metal ions are well-known as deep centers that strongly influence the electrical[1] and optical[2] properties. In general, they introduce efficient recombination channels for intrinsic excitations due to their ability to occupy different charge states.[3] In III-V semiconductors they are often used to compensate shallow impurity states in order to obtain semi-insulating material. The open-shell configuration of the transition-metal impurities is normally connected with several localized deep levels in the forbidden gap[4] and transitions between these levels are characteristic for the impurity. Thus, the detailed knowledge of the deep centers formed by $3d$ elements is a prerequisite for a complete understanding of the electrical and optical properties of real semiconductors. Additionally, intentional doping with transition metals can provide the possibility of influencing the host in a technically favorable way.

The inevitable presence of transition metals even in high-quality II-VI semiconductors is well known and contributes to the difficulties in controlling their electrical properties. A quite-common accidental contamination forming deep traps is Fe. Normally, it occupies cation lattice sites in its isoelectronic charge state Fe^{2+} giving rise to typical infrared absorption[5] and luminescence bands.[6,7] But the single-positive-charge state Fe^{3+} and the associated charge-transfer processes have also been studied by use of electron-spin-resonance (ESR) measurements.[8,9] Recently, in high-quality ZnS crystals a richly structured luminescence band around 1.0 eV has been attributed[10] to the $^4T_1(G)$-$^6A_1(S)$ transition of isolated Fe^{3+}. In ZnO, Fe-impurity centers have been detected by means of ESR (Ref. 11) but no correlated optical transitions have been reported to date.

In this paper we report on a strong and richly structured luminescence band in the red spectral region of high-quality ZnO crystals. Detailed highly resolved optical investigations in dependence on the excitation conditions, the crystal temperature, and magnetic fields up to 15 T are presented. The results lead to a straightforward identification of isolated Fe^{3+} as the luminescence center, and of the $^4T_1$-$^6A_1(S)$ transition as the luminescent one. The fine structure of the excited $^4T_1(G)$ state is discussed in the framework of an intermediate Jahn-Teller interaction. The observed transition energies and fine structure are compared with those of well-known isoelectronic d^5 configurations in II-VI semiconductors. A better understanding of the properties of d^5 configurations in very dilute systems is important regarding the technical use of semimagnetic materials.

High-resolution spectra reveal in the zero-phonon region of the Fe^{3+}($^4T_1(G)$-$^6A_1(S)$) transition additional lines that are attributed to isotope effects. Energy shifts caused by the isotope mass of the central Fe ion as well as by mass changes in the first oxygen shell are determined. Whereas isotope shifts due to the mass of the central impurity have been observed previously for several different transition-metal centers (see the references cited in Ref. 12), here the influence of the mass distribution within the first anion shell is detected. The isotope shifts are discussed in the framework of mass-dependent local phonon modes contributing to the total energy of the impurity system. The close relation to the Jahn-Teller interaction and the C_{3v} distortion of the $Fe^{3+}O^{-2}{}_4$ cluster is pointed out.

II. EXPERIMENT

The investigated samples are high-quality rods of ZnO grown in the laboratories of Professor Heiland and Pro-

 ©1992 The American Physical Society

fessor Mollwo. The crystals have dimensions in the millimeter range and have not been doped intentionally. The crystals are immersed in liquid He at temperatures about 1.8 K or in a continuous He flow of variable temperature. The photoluminescence is excited by the blue lines of a 2-W Ar^+-ion laser. Light from the crystal is decomposed in a 0.75-m double monochromator with 0.008-nm resolution and recorded with a cooled GaAs photomultiplier. The magneto-optical experiments are performed with a 15-T superconducting magnet built in split-coil geometry. For the excitation measurements, a combination of a halogen lamp and a 0.75-m double monochromator is used as a high-resolution tunable light source. In this case the luminescence is detected through a double-prism monochromator.

III. EXPERIMENTAL RESULTS

A. The luminescence

Figure 1 shows polarized emission spectra of a typical high-quality ZnO rod excited at 2.71 eV. A richly structured luminescence band is resolved. To our knowledge this luminescence is unknown in literature up to now, but its origin will be clarified in this paper. The shape of the line structure is amazingly similar to that of the prominent near-infrared luminescence[13,14] around 0.8 eV, which has been identified recently as the $^3T_2(F)$-$^3A_2(F)$ transition of isolated V^{3+}.[15] The energy positions E, the corresponding energy differences ΔE, and the predominant polarizations of the fine structure of the new luminescence are summarized in Table I. In addition, the energy differences ΔE observed in the phonon wing of the $V^{3+}(^3T_2(F)$-$^3A_2(F))$ emission are included as observed for the same crystals. Obviously, the occurring energy spacings are nearly the same in both cases; only the intensity ratios are partly changed. But in both luminescence bands the phonon replicas 7, 9, 12, 13, and 16–19 are the most striking ones. This suggests an explanation of the new luminescence as a *d-d* transition of a transition-metal center. In analogy to the V^{3+} luminescence, we interpret only the high-energy line A as a zero-phonon line (ZPL) and the whole structured sideband in terms of phonon replicas. This will be justified by the magneto-optical results presented in the following. A comparison with the phonon spectrum of the undisturbed ZnO host crystal

TABLE I. The phonon sideband of the $Fe^{3+}(^4T_1(G)$-$^6A_1(S))$ luminescence: the energy positions E, the energy differences ΔE to the ZPL A, and the favored polarizations are given. The further column gives the phonon spacings of the $V^{3+}(^3T_2(F)$-$^3A_2(F))$ luminescence as observed for the same crystal. Typical values of ZnO host phonons (Ref. 16) at distinct points of the Brillouin zone are given in the fifth column.

Line	E (eV)	ΔE (Fe^{3+}) (meV)	Polarization	ΔE (V^{3+}) (meV)	$\hbar\omega$[a] (ZnO) (meV)
A	1.787 42		∥		
1	1.774 68	12.74	—	12.6	12.5 TO(Γ)
2	1.765 16	22.26	∥	22.0	22.3 LA(A), LO(A)
3	1.757 98	29.44	⊥	28.3	
4	1.757 51	29.91	∥	30.2	30.1 TO(Γ), LO(Γ)
5	1.755 14	32.28		31.9	
6	1.753 71	33.71		33.6	
7	1.741 27	46.15	⊥	47.2	46.9 TO(Γ)
8	1.739 37	48.05	⊥	48.7	
9	1.737 92	49.50	∥	49.4	50.8 TO(Γ)
10	1.730 66	56.76	⊥	58.1	54.6 TO(Γ)
11	1.726 07	61.35		60.0	60.6 LO(Γ)
12	1.724 17	63.25	⊥	62.7	
13	1.723 78	63.64	∥	63.3	
14	1.722 67	64.75		64.9	
15	1.719 57	67.85	⊥	67.7	67.0 LO(A)
16	1.712 87	74.55	⊥	74.5	71.4 LO(Γ)
17	1.711 92	75.50		75.7	72.8 LO(Γ)
18	1.711 00	76.42		76.2	
19	1.709 90	77.52	∥	78.3	
20	1.695 30	92.12	⊥		(7)+(7)
21	1.692 00	95.42			
22	1.688 58	98.84	⊥		(9)+(9)
23	1.678 03	109.39			(7)+(12)
24	1.674 69	112.73			(9)+(12)
25	1.662 90	124.52			
26	1.660 84	126.58	∥		(12)+(12)

[a]Reference 16.

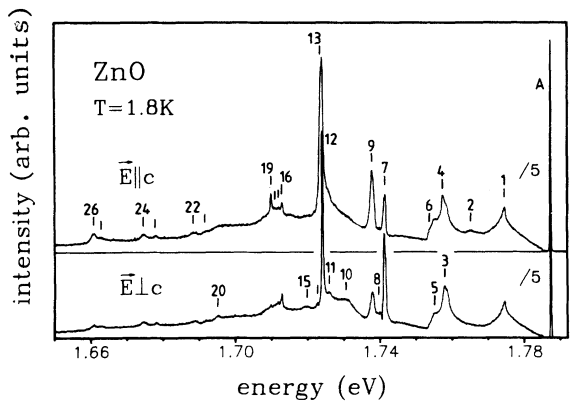

FIG. 1. Polarized luminescence spectra of a typical high-quality ZnO rod excited at 2.71 eV.

(given in the last column of Table I; the phonon energies are taken from Ref. 16) shows that the intense sharp replicas nearly correspond in their energy to optical phonons at the center of the Brillouin zone. The low-energy phonon bands represent the coupling to acoustical phonons. Additionally, combinations of the dominating phonon replica with energies of 46.1 (7), 49.5 (9), 63.25 (12), and 63.64 meV (13) occur as weak two-phonon replicas. The four phonon replicas 16–19 in the region of the upper boundary of the single-phonon density are remarkable. They are almost equally spread, separated by only 1.0 meV.

High-resolution spectra of the ZPL *A* reveal a rather complex fine structure (Fig. 2). For **E**||*c* a strong emission line at 1.787 431 eV with a full width at half maximum (FWHM) of 48 μeV dominates the spectrum. The weak line at 1.787 353 eV will later be attributed to an isotope splitting due to the natural abundance of Fe isotopes. For $E \perp c$ the intensity of the strong ZPL decreases, and a second one at 1.787 390 eV becomes visible. A decomposition of the line doublet shows that this emission has a FWHM around 50 μeV, too. Again, a further weak resonance occurs on its low-energy side.

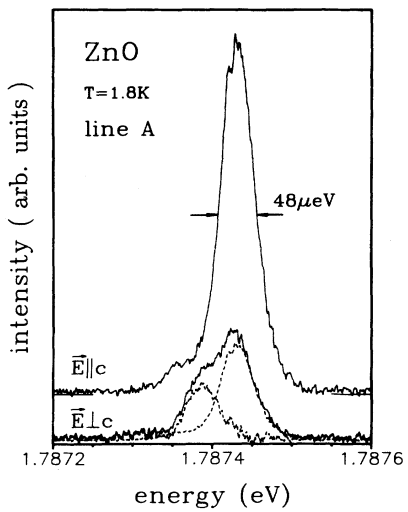

FIG. 2. Polarized spectra of the zero-phonon region of the luminescence shown in Fig. 1.

B. The ground state

In order to understand the origin of the new luminescence and to attribute the observed zero-field splitting of 41±5 μeV either to the ground or to the excited state of the luminescence, we performed magneto-optical measurements for various orientations of the crystals in magnetic fields up to 15 T. Figure 3 shows the ZPL structure *A* from Fig. 2 at $B = 5$ T for the orientations **B**||*c* and **B**⊥*c*. In both orientations six equidistant line groups are observed, each consisting of just one component for **B**||*c* and of two for **B**⊥*c*. The energy splittings between the line groups correspond to a *g* factor of about 2. The intensity ratios of the six line groups are temperature independent and therefore represent the splitting of the ground state. Only the higher-energy component of the doublets observed for **B**⊥*c* becomes stronger with increasing temperature. It represents a splitting of the excited state. The clearly resolved sixfold splitting of the ground state with a *g* factor around 2 is somewhat typical for the ^6S ground state of an electronic d^5 configuration. Obviously, an unintentionally incorporated transition metal with a d^5 configuration must be the active luminescence center under investigation.

Figure 4 shows the Zeeman behavior of the ZPL region for magnetic fields up to 5 T in the orientation **B**||*c* at low temperatures. The solid lines correspond to the Zeeman components seen in Fig. 3; those connected by dashed lines are weak and will be discussed in the framework of isotope effects in Sec. IV C. All six lines shift linearly with the magnetic field. Extrapolating all components back to zero magnetic field, they meet in three different

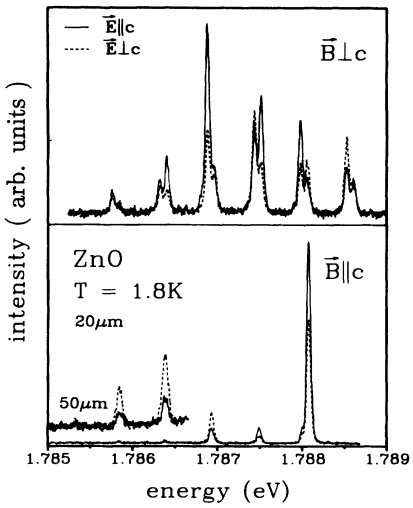

FIG. 3. Polarized luminescence spectra of the zero-phonon line region shown in Fig. 2 in a magnetic field of 5 T for the crystal orientations **B**||*c* and **B**⊥*c*. To resolve the low-energy components in the orientation **B**||*c* the slit width has been opened from 20 to 50 μm.

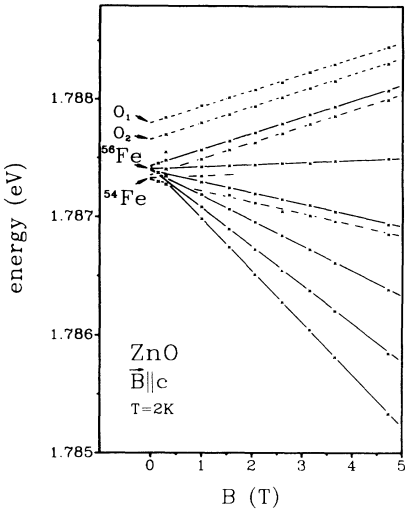

FIG. 4. Zeeman pattern of the zero-phonon region of the luminescence shown in Fig. 1, for the magnetic-field orientation $\mathbf{B}\|c$. Solid lines correspond to the dominating lines as shown in Fig. 3 attributed to ^{56}Fe in an O^{16} surrounding. Dashed lines correspond to lines shifted by isotope effects, either of the iron ^{54}Fe or of the oxygen (O_1,O_2) in the $Fe^{3+}O^{2-}{}_4$ cluster.

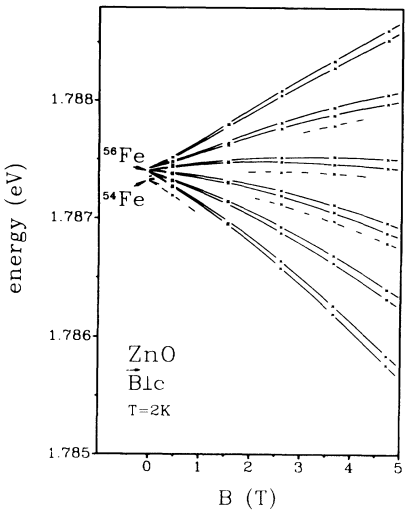

FIG. 5. Zeeman pattern of the zero-phonon region of the luminescence shown in Fig. 1, for the magnetic-field orientation $\mathbf{B}\perp c$. Solid lines correspond to the dominating lines as shown in Fig. 3 attributed to ^{56}Fe in a O^{16} surrounding. Dashed lines correspond to lines shifted by an isotope effect of the iron (^{54}Fe).

points separated by some 10 μeV, indicating a zero-field splitting of the ^6S ground state. At zero magnetic field the ^6S state is split by the spin-orbit and spin-spin interaction and the C_{3v} crystal field into three levels. S_z remains a good quantum number, and each state is twofold Kramers degenerated. A careful analysis of the Zeeman behavior of Fig. 4 shows that the averaged energies of the $\pm\frac{5}{2}$, $\pm\frac{3}{2}$, and $\pm\frac{1}{2}$ pairs are shifted and originate at 1.787 432, 1.787 399, and 1.787 389 eV, respectively. The estimated ZPL energies E and the corresponding splittings ΔE of the $^6A_1(S)$ ground state are summarized in the first part of Table II. The ZPL's shown in Fig. 2 correspond to transitions terminating at the $\pm\frac{5}{2}$ ($\mathbf{E}\|c, \mathbf{E}\perp c$) and the $\pm\frac{1}{2}$ ($\mathbf{E}\perp c$) levels; the transition to the $\pm\frac{3}{2}$ level is not resolved. The large Zeeman splittings and the narrow linewidth allow us to determine the g factor with high accuracy to

$$g_{\|,\perp}(^6A_1(S))=2.020\pm0.015\ .$$

In the orientation $\mathbf{B}\perp c$ (Fig. 5) the Zeeman behavior is nonlinear. Nevertheless, the sixfold splitting of the $^6A_1(S)$ ground state is still linear with the same g factor as in the orientation $\mathbf{B}\|c$. The twofold splittings of each line pair is linear, too.

C. The excited state

The first excited crystal-field state of a d^5 configuration in T_d symmetry is the $^4T_1(G)$ state.[17] For Mn^{2+}-impurity centers in different semiconductors this state is well known to be the luminescent one,[18] and the same holds for Fe^{3+} and ZnS.[10] The $^4T_1(G)$-$^6A_1(S)$ transition is forbidden by symmetry and spin selection rules. Thus, one of its characteristic features is a low oscillator strength. Lifetimes up to some ms are observed.[19,10] In agreement, we found a lifetime of 25.2 ms for the new luminescence

TABLE II. The zero-phonon lines of the Fe^{3+}($^4T_1(G)$-$^6A_1(S)$) luminescence: their energy positions E, the fine structure ΔE of the ground and the excited states, the favored polarizations, and the assignments of the transitions are given.

Line	E (eV)	ΔE (meV)	FWHM (μeV)	Polarization	Identification
A	1.787 432		48	∥	$\Gamma_4(\Gamma_6)\rightarrow\Gamma_4(\pm\frac{5}{2})$
	1.787 399	−0.033			$\Gamma_4(\Gamma_6)\rightarrow\Gamma_{5,6}(\pm\frac{3}{2})$
	1.787 389	−0.043	50	⊥	$\Gamma_4(\Gamma_6)\rightarrow\Gamma_4(\pm\frac{1}{2})$
B	1.788 63	1.20	100	⊥	$\Gamma_{5,6}(\Gamma_8)\rightarrow{}^6A_1(S)$
C	1.788 77	1.34			$\Gamma_4(\Gamma_8)\rightarrow{}^6A_1(S)$
D	1.790 05	2.62	140	∥	$\Gamma_4(\Gamma_7)\rightarrow{}^6A_1(S)$
E	1.791 87	4.44	1100	∥	$\Gamma_{4,5,6}(\Gamma_8)\rightarrow{}^6A_1(S)$

using a chopped Ar^+-laser excitation and a boxcar integrator. The low oscillator strength corresponding to this long lifetime makes it nearly impossible to detect the inverse absorption. Thus, most of the accessible information on the fine structure of the $^4T_1(G)$ state is revealed by temperature-dependent measurements (Fig. 6). With increasing temperature, new lines labeled *B*, *C*, *D*, and *E* emerge on the high-energy side of the ZPL *A* and are marked by arrows. At 30 K the lines *B*, *C*, and *D* become about as equally intense as the low-temperature line *A*; only line *E* remains very weak. Additionally, at 30 K all lines are shifted 100 μeV to lower energies. In the second part of Table II the extrapolated low-temperature line positions *E* are summarized; the splittings ΔE represent the fine structure of the excited $^4T_1(G)$ state.

The development of the FWHM's of the ZPL's with temperature is shown in Fig. 7. At 2 K the FWHM of at least the ZPL *A* is given by the experimental resolution; the highly resolved spectra of the same crystal (Fig. 2) reveal a FWHM of only 48 μ eV. On the other hand, the FWHM's of the transitions starting at higher excited levels are broader even at low temperatures (Table II). Additional decay channels due to relaxation within the $^4T_1(G)$ state considerably shorten the lifetimes of these states. Above 10 K the FWHM's of the ZPL's increase drastically. The solid line in Fig. 7 is a fit assuming direct phonon processes[20] between electron fine-structure levels of the $^4T_1(G)$ state. The dominating contribution is given by the interaction with the highest level separated by 4.4 meV, which appears only as a weak and broad line in the luminescence spectra (Fig. 6). For this line a low-temperature FWHM of 1.1 meV is estimated and is attributed to a fast-relaxation process due to the interaction with resonant acoustical phonons. Nevertheless, the temperature-dependent measurements show that at 2 K the ZPL *A* is inhomogeneously broadened. This indicates the absence of pure phase relaxation processes that

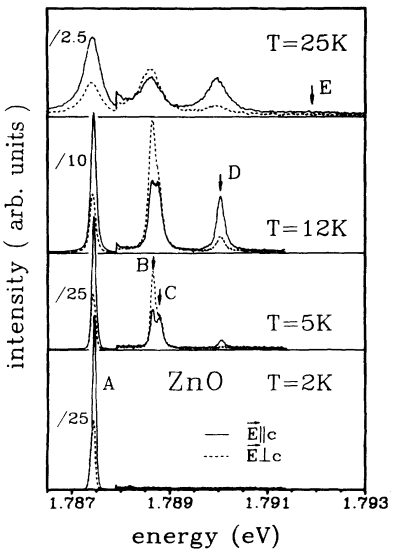

FIG. 6. Polarized luminescence spectra of a ZnO rod excited at 2.71 eV. The zero-phonon region of the luminescence described in Fig. 1 is shown for different crystal temperatures.

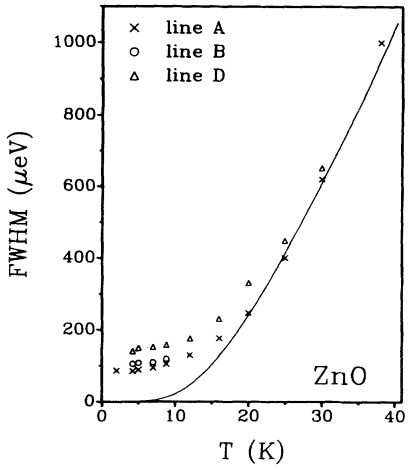

FIG. 7. Temperature dependence of the FWHM's of the ZPL's *A*, *B*, and *D*. The solid line gives a fit assuming the interaction of resonant low-frequency phonons with the electronic fine structure of the $^4T_1(G)$ state.

are fast enough to account for the linewidth.

The complete magnetic-field dependence of the excited $^4T_1(G)$ state is not accessible at present. Zeeman measurements at higher temperatures reveal complicated superpositions of six lines for each component of the excited state, which are hard to interpret with certainty. Figure 8 shows the shifts $E_m(B)$-$E_m(0)$ of the centers of gravity of associated sixfold splittings as observed at $T=2$ K (Figs. 4 and 5). For the orientation $\mathbf{B}\|c$ just one excited state is observed, shifting linearly to lower energies, with -159 μeV/T. Under the assumption of a $S_z=-\frac{3}{2}$ level this corresponds to a *g* factor of

$$g_{\|}^{e}=1.83\ .$$

In the orientation $\mathbf{B}\perp c$ a splitting of the lowest excited state into two components is observed. This splitting is linear over the whole investigated magnetic field range up to 15 T, with

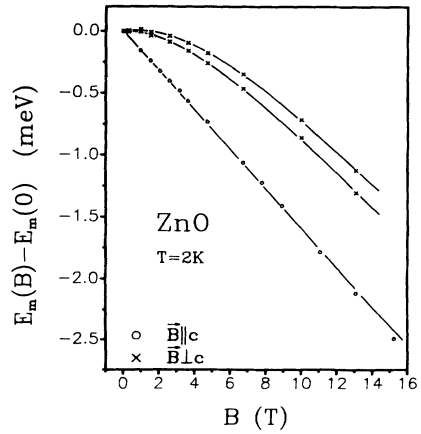

FIG. 8. Magnetic-field dependence of the lowest excited state in the orientations $\mathbf{B}\|c$ and $\mathbf{B}\perp c$. The center of gravity of the $^6A_1(S)$ state is assumed to be independent of the magnetic field.

$g_{\perp}^{e}=0.27\pm0.02$.

The mean energy of this splitting does not shift below 1.5 T but starts to shift to lower energies above. Above 10 T the slope of this shift reaches the one observed for $\mathbf{B}\|c$. Obviously, the Zeeman behavior of the excited state is dominated by the spin-dependent parts of the Hamilton operator. The small splitting is probably caused by the orbital part.

D. The excitation

Figure 9 shows the excitation spectrum of the luminescence on a logarithmic scale. The spectra are recorded using low excitation densities provided by a halogen lamp in combination with a double-grating monochromator as tunable light source. No resonant excitation in the red spectral region is observed. On the low-energy side the excitation has its onset at 2.25 ± 0.05 eV and increases more than three orders of magnitude in efficiency towards the band gap. Broad excitation maxima are found at 3.08 eV ($\mathbf{E}\perp c$) and 3.11 eV ($\mathbf{E}\|c$). At higher energies the excitation efficiency decreases again. Absorption measurements of the same crystals show that this decrease coincides with an increasing absorption of the crystal. The luminescence intensity is thereby limited by the decrease of the excited volume of the crystal, which is connected with a decrease of accessible luminescence centers. The minima of the excitation efficiency at 3.382 eV ($\mathbf{E}\perp c$) and 3.422 eV ($\mathbf{E}\|c$) correspond in energy and polarization to the free A, B, and C excitons,[21] respectively, as indicated in Fig. 9. On their high-energy sides additional minima appear due to the formation of excited excitonic states.

Exciting with the blue and green lines of a cw Ar^{+}-ion laser with excitation densities up to a few W cm^{-2}, a saturation of the luminescence intensity is observed. Figure 10 shows the development of the luminescence intensity

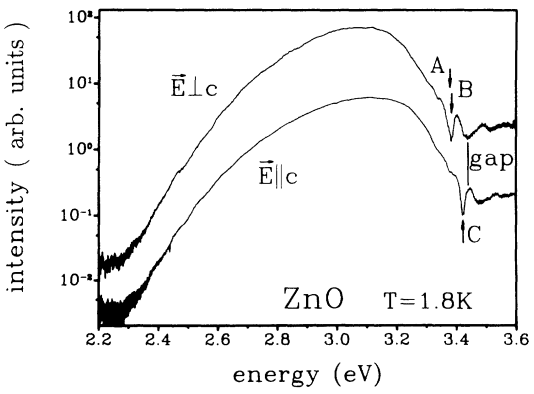

FIG. 9. Polarized excitation spectra of the luminescence shown in Fig. 1. Low excitation densities as provided by a halogen lamp in combination with a double-grating monochromator have been used. The luminescence is detected through a double-prism monochromator set to 1.724 eV. The energy positions of the free A, B, and C excitons and the band gap are marked.

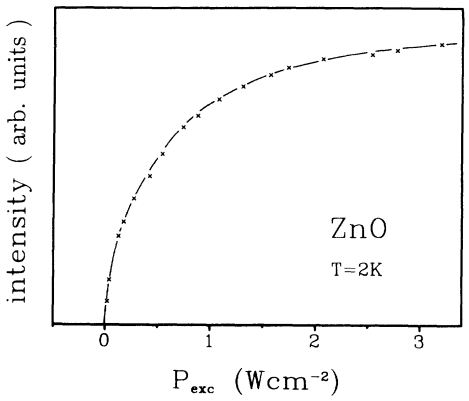

FIG. 10. Saturation of the luminescence intensity with the excitation density of the 2.71-eV line of a cw Ar^{+}-ion laser.

recorded with the 2.71-eV line. The saturated luminescence intensity increases with increasing excitation energy. At higher energies new excitation channels open up. Therefore, the broad visible excitation band must be composed out of different overlapping contributions and cannot be connected with the luminescence center alone. The saturation is not caused by the finite number of luminescence centers, but rather by a saturation of the excitation channels. The excitation channels saturate due to the long (25.2 ms) storage of the excitation energy in the $^{4}T_{1}(G)$ state. The luminescence center has to be excited by energy-transfer processes starting at other impurities. Such an excitation process is well established for the Fe^{3+} center in ZnS,[10] which is excited by the recombination of photogenerated free holes with Fe^{2+} centers. The $Cu^{2+}\rightarrow Cu^{+}+h_{VB}$ charge-transfer process has been identified as the dominating source for the holes. Here, for this luminescence, the type of the energy transfer as well as the sources are still unclear.

Excitation measurements with high-intensity pulses of 15-ns duration of an excimer laser-pumped dye laser with a repetition rate of 60 Hz do not reveal resonant excitation resonances either, but show excitation below the low-energy threshold at 2.25 eV observed in the cw experiments. Figure 11 shows the luminescence intensity with the pulsed excitation densities in a double logarithmic plot. Exciting at 2.30 eV above the low-energy threshold, a linear dependence is observed with beginning saturation around 10 MW cm^{-2}, demonstrating the one-photon character of the excitation process at this energy. The saturation threshold of 10 MW cm^{-2} is substantially higher than in cw experiments, but the averaged cw excitation densities are in both cases in the order of 1 W cm^{-2}. The 25.2-ms lifetime of the excited state leads to an accumulation of excited luminescence centers in cw experiments, which here recovers between two pulses. Exciting below the threshold at 2.18 or 2.10 eV, a superlinear behavior is observed, where the luminescence intensity is lower than after excitation above the threshold. Exciting at 2.10 eV, a nearly quadratic dependence occurs, indicating two-photon band-band absorption. Thus, it is shown that the luminescence center can be ex-

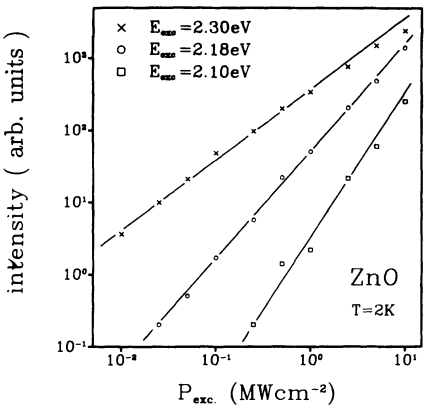

FIG. 11. Double logarithmic plot of the intensity of the luminescence shown in Fig. 1 with the excitation density for different excitation energies, using 15-ns pulse of an excimer laser-pumped dye laser.

cited by the recombination of photogenerated free carriers.

IV. DISCUSSION

A. The chemical nature of the luminescence center

The observed sixfold Zeeman splitting with a g factor of 2.020 ± 0.015 leads to an unambigious identification of the ground state as the $^6A_1(S)$ state of an electronic d^5 configuration. Taking into account that the first excited state of the d^5 configuration is the $^4T_1(G)$ level, the luminescence is attributed to the $^4T_1(G)$-$^6A_1(S)$ transition. Further, the luminescence center has to be a point defect excluding associates or structural defects; otherwise, no distinct polarization with respect to the c axis of the hexagonal ZnO crystal would be expected. Among the transition metals are three possible candidates (Cr^+,Mn^{2+},Fe^{3+}) for the luminescence center with a d^5 configuration. The g factors of all three candidates are expected to be around 2, but only the Mn^{2+} and Fe^{3+} centers are known from ESR in ZnO.[22,11] Though the g factors are equal within the experimental error of the magnetoluminescence measurements, the observed g factor of 2.020 gives a hint favoring Fe^{3+}, which has the largest one. The $^6A_1(S)$ ground state is split threefold in zero magnetic field by the combined action of second-order spin-orbit and spin-spin interaction and the C_{3v} crystal field. From ESR results the corresponding fine-structure splittings can be calculated. This splittings are also resolved in the present magneto-optical investigation, giving a clear identification of the luminescence center.

The fine structure and Zeeman behavior of the $^6A_1(S)$ state are described by the following spin Hamiltonian:[23]

$$H=g\mu_B\mathbf{H}\cdot\mathbf{S}+(a/6)[S_\xi^4+S_\eta^4+S_\zeta^4-707/16]+D(S_z^2-35/12)+(7F/36)[S_z^4-(95/14)S_z^2+81/16] .$$

The axial symmetric component of the C_{3v} crystal field, which is given by the terms proportional to D and F, lies within the z axis, the c axis of the hexagonal ZnO crystal. This axis corresponds to a [111] axis in the cubic system given by ξ, η, and ζ, in which the cubic part of the crystal field is defined proportional to a. Figure 12 shows the fine structure of the $^6A_1(S)$ state of isolated Fe^{3+} in a magnetic field for the orientation $\mathbf{B}\|c$, calculated with the following parameters determined in ESR experiments for ZnO:[24]

$$D=-7.38\ \mu\text{eV} ,$$
$$a-F=0.46\ \mu\text{eV} ,$$
$$|a|=0.51\ \mu\text{eV} ,$$
$$g=2.0062 .$$

The absolute sign of the used parameters is difficult to obtain by ESR but is chosen to fit our magneto-optical results. For Fe^{3+} (Mn^{2+}), the zero-field splittings between the $\pm\frac{5}{2}$ ground state and the $\pm\frac{3}{2}$ and $\pm\frac{1}{2}$ states amount to 32.515 μeV (11.798 μeV) and 44.120 μeV (17.546 μeV), respectively. The corresponding parameters of Cr^+ are unknown as of yet due to the still-missing ESR signal. The $-\frac{1}{2}$ and the $+\frac{5}{2}$ as well as the $+\frac{1}{2}$ and the $-\frac{5}{2}$ components experience a term interaction due to the cubic term proportional to a of the Hamilton operator. This leads to a nonlinear Zeeman behavior. But this interaction, which prohibits the crossing of the participating states, is weak and can be neglected in the analysis of our magneto-optical results. Thus, in a magnetic field the zero-field splitting occurs as a shift of the averaged energies of the $\pm\frac{1}{2}$, $\pm\frac{3}{2}$, and $\pm\frac{5}{2}$ components, respectively. Analyzing the Zeeman data given in Fig. 4, the mean energy of the $\pm\frac{5}{2}$ components is found at highest energies, and those of the $\pm\frac{3}{2}$ and $\pm\frac{1}{2}$ components are shifted 33 ± 4 and 43 ± 4 μeV to lower energies, respectively. The

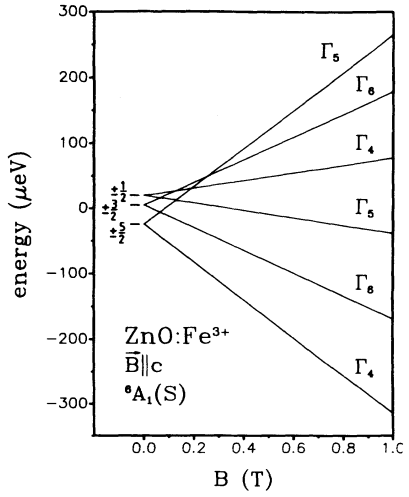

FIG. 12. Calculated fine structure of the $^6A_1(S)$ state of isolated Fe^{3+} in ZnO in a magnetic field with $\mathbf{B}\|c$. The parameters used are taken from ESR results (Ref. 24).

extrapolated zero-field energies are summarized in Table II. The zero-field splitting of the luminescence ground state is in excellent agreement with that calculated from ESR data of Fe^{3+} (Fig. 12), proving the nature of the luminescence center. Additionally, the absolute signs of the parameters used are determined. The trigonal splitting parameter D is negative.

The two ZPL's observed at zero magnetic field (Fig. 2) correspond in their energies to transitions from the lowest excited state to the $\pm\frac{1}{2}$ and $\pm\frac{5}{2}$ components of the $^6A_1(S)$ ground state, respectively. Their energy separation of 41 ± 5 μeV agrees well with the splitting between the $\pm\frac{1}{2}$ and $\pm\frac{5}{2}$ components determined in the magneto-optical measurements. The example of ZnO:Fe^{3+} as well as of ZnO:V^{3+} (Ref. 15) and ZnO:Ni^{3+} (Ref. 25) show impressively that the connection of ESR and high-resolution magneto-optical results can lead to clear identifications of luminescence transitions.

Luminescence of additional Fe^{3+} centers in II-VI semiconductors is only reported for ZnS,[10] where a richly structured luminescence band is found in the near-infrared spectral region around 1.0 eV. Comparing the $^4T_1(G)$-$^6A_1(S)$ transition energies of the Fe^{3+} centers with the energy difference ^4G-^6S of the free ion of 4.07 eV,[26] a strong covalent reduction of the Racah parameters B and C can be stated. Comparable effects have been observed for Fe^{3+} centers in other materials. The $^4T_1(G)$-$^6A_1(S)$ transition energies of $FeCl_4^-$ and of the Fe-S center in rebredoxin are reduced to 44% (Refs. 26 and 27) and 65%,[27] respectively. As expected, the covalent reduction is stronger in ZnS (25%) than in ZnO (44%), since the first one is the more-covalent host. The influence of the different local bonding properties in both semiconductors is revealed in the observed luminescence lifetimes, too. The electric dipole transitions become allowed mainly by the admixture of odd-parity states of the ligands to the d-like impurity states by the covalent bonding or the spin-orbit interaction with the ligands.[28] In good agreement, the oscillator strength of the $^4T_1(G)$-$^6A_1(S)$ transition in ZnS (7.9×10^{-6}) is about 20 times larger than in the more ionic ZnO (3.8×10^{-7}).

ESR spectra of the investigated ZnO crystals show the presence of Fe^{3+} centers above 77 K, but not at lower temperatures. Therefore, the lack of the absorption and resonant excitation of the $^4T_1(G)$-$^6A_1(S)$ transition is not only caused by its extremely low oscillator strength but also by the lack of Fe^{3+} centers in the unexcited crystal. At low temperatures the unexcited charge state is probably the isoelectronic Fe^{2+}, and after excitation Fe^{3+} arises in its excited $^4T_1(G)$ state. It is unlikely that the direct charge-transfer process

$$\begin{aligned}Fe^{2+}+\hbar\omega_{blue}&\rightarrow Fe^{3+}(^4T_1(G))+e_{CB}\\&\rightarrow Fe^{3+}(^6A_1(S))+e_{CB}+\hbar\omega_{red}\end{aligned}$$

can explain the low-energy threshold in the excitation spectra (Fig. 9). The excitation energy needed would be the $^4T_1(G)$-$^6A_1(S)$ transition energy of 1.79 eV plus the photoionization energy of the Fe^{2+} center, which should exceed by far the low-energy threshold at 2.25 eV. Moreover, the intensity-dependent measurements show that the saturation is not due to the limited number of Fe centers. Obviously, the luminescence is excited by energy-transfer processes from as yet unidentified defects (deep acceptors labeled A^0) to Fe^{2+} centers by photogenerated holes:

$$\begin{aligned}Fe^{2+}+A^0+\hbar\omega_{blue}&\rightarrow Fe^{2+}+A^-+h_{VB}\\&\rightarrow Fe^{3+}(^4T_1(G))+A^-\\&\rightarrow Fe^{3+}(^6A_1(S))+A^-+\hbar\omega_{red}\ .\end{aligned}$$

This is basically the same mechanism as that described in Ref. 29 for the system ZnS:Fe^{3+}, but this time the hole sources are not yet identified. The low-energy onset at 2.25 eV gives a lower limit for the ionization energies of these deep acceptors. Subsequently, the Fe^{3+} centers serve as hole sources themselves.

B. The fine structure of the $^4T_1(G)$ state

Information about the fine structure and the phonon coupling in the excited $^4T_1(G)$ state is obtained from temperature-dependent measurements (Fig. 6). The observed fine structure consisting of at least five states is somewhat strange for the $^4T_1(G)$ state of an electronic d^5 configuration. In general, a strong Jahn-Teller interaction with E modes leads to a reduction of the electronic fine structure to a twofold splitting by second-order interactions.[30] In the case of a weak or intermediate coupling, a fourfold structure is expected due to the spin-orbit interaction, which is in good agreement with the observed four main line groups. Only for the first excited state is an additional splitting into the lines B and C by the C_{3v} crystal field resolved. The resulting term scheme is given in Fig. 13. The spin-orbit interaction, the spin-spin interaction, an intermediate Jahn-Teller interaction, and the C_{3v} crystal field have to be considered to explain the fine structure. The energy splittings ΔE as well as the energies E of the high-temperature emission lines are summarized in Table II. The Zeeman measurements show that the lowest excited state is a doublet. Thus, it is attributed to the $\Gamma_4(\Gamma_6)$ state. The two excited states shifted by 1.22 and 1.36 meV to higher energies are attributed to the $\Gamma_{5,6}$ and Γ_4 components of the first excited Γ_8 state, respectively (see Fig. 13). The lower one is associated with the $\Gamma_{5,6}$ state, since the polarization of the emission starting at this level is opposite to that starting at the lowest $\Gamma_4(\Gamma_6)$ state. The next state shifted by 2.62 meV is attributed to the $\Gamma_4(\Gamma_7)$ state. The polarization of line D starting at this level is comparable to that of the low-temperature line A. The state shifted by 4.40 meV is attributed to the unresolved $\Gamma_{4,5,6}$ components of the second Γ_8 state. The C_{3v} splitting is not resolved because of the large FWHM of 1.1 meV of the corresponding emission line. Detailed magneto-optical investigations of the fine structure of the $^4T_1(G)$ state by means of excitation spectroscopy would provide interesting information about this system, which exhibits just a relatively weak Jahn-Teller interaction.

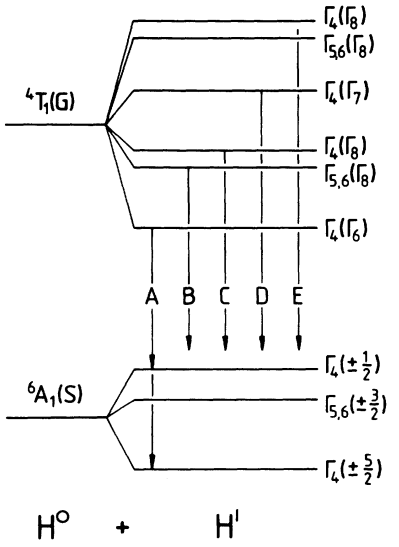

FIG. 13. Simplified term scheme of Fe^{3+}. H^0 contains the interelectronic Coulomb interaction and the T_d crystal field, H' contains the spin-orbit interaction, the spin-spin interaction, the C_{3v} crystal field, and an intermediate Jahn-Teller interaction with E modes. The observed ZPL's are represented by arrows. The spacings are not given on a unique energy scale.

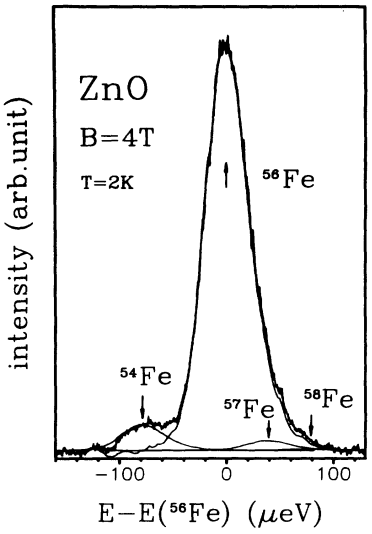

FIG. 14. The highest-energy component of the ZPL A in a magnetic field of 5 T and the orientation $\mathbf{B}\|c$. The line shape is fitted by equal line shapes for each Fe isotope regarding a linear isotope shift of 39 μeV/nucleon and their natural abundance.

C. Isotope effects

Looking back to the high-resolution picture Fig. 2 or the Zeeman data in Fig. 4, it is obvious that the situation is more complicated than outlined above. Additional lines are visible in addition to those discussed. Figure 2 reveals for each strong line a weaker partner on its low-energy side with less than a tenth of its intensity. The Zeeman data represented in Figs. 4 and 5 show these weak lines (marked at zero magnetic field with ^{54}Fe) shifting just like the dominating components previously discussed. Due to the threefold zero-field splitting of the $^6A_1(S)$ state, the zero-field spectra are very complex. Nevertheless, the electronic degeneracies of the ground and excited states are completely lifted in a magnetic field. The line shape of the strongest component of ZPL A at $B=4$ T in the orientation $\mathbf{B}\|c$ is decomposed into four lines assuming linear isotope shifts and the natural abundance of Fe isotopes (Fig. 14). The dominating line is attributed to the ^{56}Fe isotope with an abundance of 91.7%, while the low-energy line belongs to the isotope ^{54}Fe with an abundance of 5.8%. The contributions of the ^{57}Fe (2.2%) and the ^{58}Fe (0.3%) isotopes are too weak to be resolved in the spectra. The isotope shift amounts to 39±3 μeV/nucleon and is positive; i.e., the transition energy increases with increasing isotope mass. The isotope shift is found to be independent of the magnetic field within the margins of experimental error.

To explain isotope shifts of transition-metal centers in semiconductors in the order of some 10 μeV/nucleon, the mass dependence is attributed to the phonon system.[12] Each phonon mode contributes with at least its zero-point energy to the total energy E_t of the impurity system in a given electronic state. Therefore, in principle, each mass-dependent phonon mode contributes to the mass dependence dE_t/dm. Isotope shifts observed for optical transitions can be understood on the basis of different mass dependencies of the total energies of the impurity system in the ground and excited electronic states:

$$(dE/dm)_{\text{transition}}=(dE_t/dm)_e-(dE_t/dm)_g \ . \qquad (1)$$

(e) represents the excited state and (g) the ground state of the impurity system, which are connected by the optical transition under consideration.

To understand the isotope shifts, the problem can be split in two parts: first, the mass dependencies $d\hbar\omega_i/dm$ of the phonon modes $\hbar\omega_i$, and second, the dependencies $dE_t/d\hbar\omega_i$ of the total energy of the impurity system in a given electronic state on the phonon modes $h\omega_i$ must be evaluated. This is expressed by the following formula:[12]

$$dE_t/dm=\sum_i (dE_t/d\hbar\omega_i)(d\hbar\omega_i/dm) \ . \qquad (2)$$

The summation includes the whole phonon system, but only the mass-dependent phonon modes ($d\hbar\omega_i/dm\neq 0$) give nonvanishing contributions. A measure for the derivation $d\hbar\omega/dm$ is the contribution of the motion of the impurity ion to the energy of the phonon mode. Thus, only local modes with their strong localization around the impurity ion are expected to depend on the impurity mass. In particular, considering the next neighbors in a tetrahedral cluster, only modes with T_2 symmetry move the central ion.[31] However, in each concrete case the local phonon system needs a careful analysis. The mass dependence of the local modes can be calculated[12] within the Keating valence force model[32] using local mode energies determined, e.g., by Raman spectroscopy.[33] However, it is expected that their mass dependence

$d\hbar\omega/dm$ is negative, i.e., the phonon energy decreases with increasing isotope mass.

The dependence $dE_t/d\hbar\omega$ of the total energy of an impurity center on the phonon energy is, in general, larger than zero. If the phonon mode of interest is not subject to an electron-phonon coupling, then it contributes $(N+G/2)\hbar\omega$ to the total energy E_t and $dE_t/d\hbar\omega$ becomes $(N+G/2)$, where G is the degeneracy of the phonon mode ($G=3$ for a T_2 mode). This is altered if the phonon mode couples to the electronic state via a Jahn-Teller effect, forming vibronic states. In this case $dE_t/d\hbar\omega$ becomes smaller than $G/2$, at least for the vibronic ground state.

To observe an isotope effect in an optical transition, dE_t/dm has to be different in the excited and ground states. Since in both states, in general, the phonon system is basically the same, either the phonon frequencies are shifted due to different force constants (frequency effect) or a mass-dependent phonon mode is subject to a noticeable Jahn-Teller interaction in at least one of the states. The first effect is expected to be small if two $3d$ states are considered, but becomes important if charge-transfer processes are involved. In the second case $dE_t/d\hbar\omega$ can be different in both states, and from Eqs. (1) and (2) it follows that

$$(dE/dm)_{\text{transition}} = \sum_i [(dE_t/d\hbar\omega_i)_e - (dE_t/d\hbar\omega_i)_g]d\hbar\omega_i/dm \ . \quad (3)$$

The summation includes all mass-dependent phonon modes.

In the case of ZnO:Fe^{3+}, the excited $^4T_1(G)$ state is Jahn-Teller active, which results in a smaller mass dependence than that of the $^6A_1(S)$ ground state. A positive isotope shift dE/dm is expected for the $^4T_1(G)$-$^6A_1(S)$ transition, in good agreement with the experiment. Thus, the isotope shift demonstrates that in the excited $^4T_1(G)$ state at least one mass-sensitive local mode experiences a noticeable Jahn-Teller interaction. At first sight this would imply the action of T_2 modes. However, in fine-structure calculations of the $^4T_1(G)$ state, normally E modes are considered.[30] But the C_{3v} crystal field can cause a mixing of the E modes with the mass-sensitive T_2 modes.

In the framework of the above discussion, it becomes clear that the isotope effect can depend on the C_{3v} crystal field, as is stated in literature.[34] This should be the case if the Jahn-Teller active phonon is of the E type. If the T_2 modes are Jahn-Teller active, as in the case of the Ni^{2+}($^3T_1(F)$-$^3T_1(P)$) transition,[35] no effect is expected. Indeed, a very recent investigation[36] of the ZnS:Ni^{2+} system revealed almost equal isotope shifts for the cubic as well as the trigonal distorted centers. Similar considerations also hold for other systems, like ZnO:Ni^{3+}. For the Ni^{3+}($^4T_2(F)$-$^4A_2(F)$) transition a positive isotope shift of 13.5 μeV/nucleon is found,[25] and again only the excited $^4T_2(F)$ state is subject to a Jahn-Teller interaction.

Figure 15 shows the zero-phonon region of the $^4T_1(G)$-$^6A_1(S)$ luminescence at 2 and 4.2 K. On the high-energy side of the ZPL A, two additional emission lines appear shifted by 222 (O_2) and 365 μeV (O_1) to higher energies. They show the same polarization behavior and just $0.63\pm0.05\%$ and $0.18\pm0.05\%$ of the intensity of the ZPL A. The intensity ratios do not depend on the investigated crystal or on the crystal temperature. The Zeeman behavior is the same, too, at least as far as it is observed (Fig. 4). The whole behavior indicates further Fe^{3+} centers from these emission lines, which are just shifted slightly in energy. A similar behavior has been observed for ZnS:Fe^{3+} and attributed to the polytypic crystal structure of ZnS.[10] For ZnO the hexagonal phase is very stable and no polytypes have been reported up to now. Additionally, different crystals exhibit the same intensity ratios, which excludes structural imperfections of the crystals or possible associates. On the other hand, the line pattern looks like an isotope splitting, but, as stated above, the isotope shift induced by the Fe ion is much smaller.

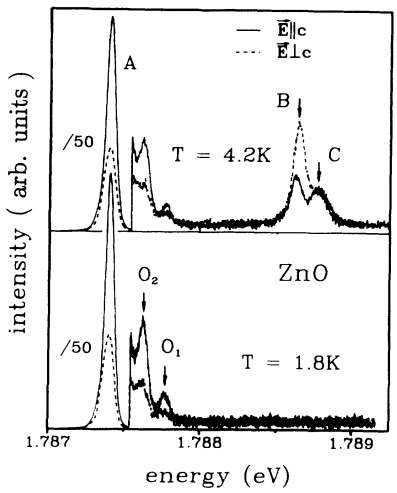

FIG. 15. Polarized luminescence spectra of the ZPL region at 1.8 and 4.2 K excited with the 2.71-eV line of an Ar^+-ion laser. The weak lines marked by O_1 and O_2 are shifted with respect to the dominating ZPL A by the presence of one O^{18} ion in the $Fe^{3+}O^{2-}{}_4$ cluster.

Not only the motion of the impurity ion, but also that of the ions in its nearest neighborhood contribute to the energy of a local phonon. Thus, a local phonon can be sensitive to the mass of the ligands of the impurity ion, too, possible causing a further isotope shift of a d-d transition of the impurity. Oxygen has three stable isotopes: O^{16} (99.762%), ^{17}O (0.038%), and ^{18}O (0.200%). Simple statistical considerations show that the probability of finding only ^{16}O ions in the $Fe^{3+}O_4{}^{2-}$ cluster is about 99.051%, and of finding one ^{18}O ion is 0.795%. In the hexagonal ZnO crystal the $Fe^{3+}O_4{}^{2-}$ cluster is distorted, and only the three off-axis O places remain equivalent. The probability of finding the ^{18}O ion in the direction of the c axis is 0.199%, and the probability of finding it on an off-axis place is 0.596%. In the last case, $Fe^{3+}O_4{}^{2-}$ clusters with one ^{17}O ion in the direction of the c axis are expected to contribute about 0.038%, too, which is not

resolved in the spectra. These statistical weights are in excellent agreement with the intensity ratios shown in Fig. 15. Additionally, the line shape used to fit the Fe-isotope splitting in Fig. 14 is only almost of Gaussian shape, but is slightly distorted on its high-energy side. In the present framework this distortion can be attributed to the isotope shift induced by ^{18}O in the second oxygen shell. The observed mass dependence is again positive, in agreement with the Fe-induced isotope shift.

The isotope effect induced by oxygen is larger than the one induced by Fe. There are many possible reasons to account for this effect. The relative mass difference is larger for oxygen ($\sim 6\%$/nucleon) than for Fe ($\sim 1.8\%$/nucleon). T_2 modes are especially sensitive to the Fe mass, but all modes can be sensitive to the oxygen mass. This can be of particular interest if only E modes experience a noticeable Jahn-Teller interaction, as in the investigated system. Moreover, simply the contribution of an oxygen ion to the mass dependence of a distinct local phonon can be larger than that of the Fe ion.

V. CONCLUSION

In the present paper the luminescence properties of high-quality ZnO crystals are investigated. A richly structured luminescence appearing around 690 nm under blue excitation is found. On the basis of detailed magneto-optical results, this luminescence is interpreted as the $^4T_1(G)$-$^6A_1(S)$ transition of isolated Fe^{3+} ions on Zn^{2+} lattice sites. Basic arguments are the sixfold splitting in a magnetic field with a g factor of 2.020 ± 0.015 and the threefold zero-field splitting of the ground state. This example demonstrates how powerful a combination of magneto-optical measurements and ESR can be in analyzing optical spectra of distorted semiconductors.

The excitation of the Fe^{3+}($^4T_1(G)$-$^6A_1(S)$) luminescence takes place by an energy transfer through photogenerated free holes from deep acceptors to Fe^{2+} centers. The participating acceptor centers have binding energies larger than 2.25 ± 0.05 eV. Saturation of the luminescence intensity occurs even under cw excitation, which is caused by the 25.2-ms lifetime of the excited $^4T_1(G)$ state. Five fine-structure levels are found for the $^4T_1(G)$ state, indicating just an intermediate Jahn-Teller interaction. Obviously, the C_{3v} crystal field stabilizes the Fe^{3+} center against E-type distortions, giving interesting topics for further theoretical considerations.

Two different isotope shifts are observed: Fe isotopes shift the transition energy by 39 μeV/nucleon, and the presence of one O^{18} isotope among the O^{16} ions in the $Fe^{3+}O^{2-}{}_4$ cluster shifts the transition energy by 365 or 222 μeV, depending on its location. The isotope shifts are interpreted in terms of local phonon modes, which are sensitive to the mass distribution in the $Fe^{3+}O^{2-}{}_4$ cluster. It is pointed out that in order to observe an isotope shift in an optical transition, at least one mass-dependent local phonon mode has to experience a Jahn-Teller interaction either in the ground or excited state. Therefore, isotope effects give valueable hints for fine-structure calculations involving the electron-phonon interaction. The experimental data presented challenge the detailed consideration of the local phonon system of impurity centers formed by an isolated transition-metal ion. This holds especially for the O-induced isotope shift, which is unique for such a center in a II-VI semiconductor.

ACKNOWLEDGMENTS

This work has been supported partly by the Deutsche Forschungsgemeinschaft (Bonn, Germany). The authors wish to thank Professor Mollwo and Professor Heiland for supplying the vapor-grown undoped ZnO crystals.

[1]R. H. Bube, *Photoconductivity of Solids* (Wiley, New York, 1960).
[2]H. A. Weakliem, J. Chem. Phys. **36**, 2117 (1962).
[3]J. W. Allen, J. Phys. C **2**, 1077 (1969).
[4]J. M. Langer and H. Heinrich, Phys. Rev. Lett. **55**, 1414 (1985).
[5]G. A. Slack, F. S. Ham, and R. M. Chrenko, Phys. Rev. **152**, 376 (1966).
[6]F. S. Ham and G. A. Slack, Phys. Rev. B **4**, 777 (1971).
[7]M. Skowronski and Z. Liro, J. Lumin. **24/25**, 253 (1981).
[8]R. S. Title, Phys. Rev. **131**, 623 (1963).
[9]M. Godlewski and A. Zakrzewski, J. Phys. C **18**, 6615 (1985).
[10]A. Hoffmann, R. Heitz, and I. Broser, Phys. Rev. B **41**, 5806 (1990).
[11]W. M. Walsh and L. W. Rupp. Phys. Rev. **126**, 952 (1962).
[12]A. Hoffmann and U. Scherz, J. Cryst. Growth **101**, 385 (1990).
[13]P. J. Dean, D. J. Robbins, S. G. Bishop, J. A. Savage, and P. Porteous, J. Phys. C **14**, 2847 (1981).
[14]C. West, D. J. Robbins, P. J. Dean, and W. Hayes, Physica B **116**, 492 (1983).
[15]R. Heitz, A. Hoffmann, B. Hausmann, and I. Broser, J. Lumin. **48/49**, 689 (1991).
[16]H.-J. Schulz and M. Thiede, Phys. Rev. B **35**, 18 (1987).
[17]J. S. Griffith, *The Theory of Transition-Metal Ions* (Cambridge University, London, 1971).
[18]H.-E. Gumlich, J. Lumin, **23**, 73 (1981).
[19]W. Busse, H.-E. Gumlich, A. Geoffroy, and R. Parrot, Phys. Status Solidi B **93**, 591 (1979).
[20]B. Di Bartolo, in *Optical Interactions in Solids* (Wiley, New York, 1968), Ch. 15.
[21]*II-VI and III-V Compounds*, edited by O. Madelung, Landolt-Börnstein, New Series, Group X, Vol. 17b, Pt. 37 (Springer-Verlag, Berlin, 1982).
[22]J. Schneider and S. R. Sircar, Z. Naturforsch. A **17**, 570 (1962).
[23]B. Bleaney and R. S. Trenam, Proc. Soc. London, Ser. A **223**, 1 (1954).
[24]J. Schneider, Z. Naturforsch. A **17**, 189 (1962).
[25]P. Thurian, R. Heitz, A. Hoffmann, and I. Broser, Proceedings of the 5th II-VI Compounds Conference 1991, Tamano, Japan [J. Cryst. Growth (to be published)].

[26]C. K. Jörgenson, Discuss. Faraday Soc. **26**, 110 (1958).
[27]J. C. Deaton, M. S. Gebhard, S. A. Koch, M. Millar, and E. I. Solomon, J. Am. Chem. Soc. **110**, 6241 (1988).
[28]D. Boulanger, D. Curie, and R. Parrot, J. Lumin **48/49**, 680 (1991).
[29]R. Heitz, A. Hoffman, P. Thurian, and I. Broser, J. Phys. Condens. Matter **4**, 157 (1992).
[30]P. Koidl, Phys. Status Solidi B **74**, 477 (1976).
[31]R. Engelman, *The Jahn-Teller Effect in Molecules and Crystals* (Wiley-Interscience, London, 1972).
[32]P. N. Keating, Phys. Rev. **145**, 637 (1966).
[33]M. Zigone, M. Vandevyver, and D. N. Talwar, Phys. Rev. B **24**, 5763 (1981).
[34]B. Clerjaud, D. Côte, F. Gendron, M. Krause, and W. Ulrici, Mater. Sci. Forum **38-41**, 775 (1989).
[35]B. Nestler, A. Hoffmann, L. B. Xu, U. Scherz, and I. Broser, J. Phys. C **20**, 4613 (1987).
[36]R. Heitz, A. Hoffmann, and I. Broser (unpublished).